THE FASEB JOURNAL • RESEARCH • www.fasebj.org

Altered methylation of specific DNA loci in the liver of *Bhmt*-null mice results in repression of *Iqgap2* and *F2rl2* and is associated with development of preneoplastic foci

Daniel S. Lupu,[*] Luz D. Orozco,[†] Ying Wang,[‡] John M. Cullen,[§] Matteo Pellegrini,[†] and Steven H. Zeisel[*,1]

[*]Department of Nutrition, Nutrition Research Institute, University of North Carolina at Chapel Hill, Kannapolis, North Carolina, USA; [†]Department of Molecular, Cell, and Developmental Biology, University of California, Los Angeles, Los Angeles, California, USA; [‡]Department of Clinical Nutrition, School of Medicine, Xin Hua Hospital, Shanghai Jiao Tong University, Shanghai, China; and [§]North Carolina State University, College of Veterinary Medicine, Raleigh, North Carolina, USA

ABSTRACT: Folate B_{12}–dependent remethylation of homocysteine is important, but less is understood about the importance of the alternative betaine-dependent methylation pathway—catalyzed by betaine-homocysteine methyltransferase (BHMT)—for establishing and maintaining adequate DNA methylation across the genome. We studied C57Bl/6J *Bhmt* (betaine-homocysteine methyltransferase)-null mice at age 4, 12, 24, and 52 wk ($N = 8$) and observed elevation of *S*-adenosylhomocysteine concentrations and development of preneoplastic foci in the liver (increased placental glutathione *S*-transferase and cytokeratin 8-18 activity; starting at 12 wk). At 4 wk, we identified 63 differentially methylated CpGs (DMCs; false discovery rate < 5%) proximal to 81 genes (across 14 chromosomes), of which 18 were differentially expressed. Of these DMCs, 52% were located in one 15.5-Mb locus on chromosome 13, which encompassed the *Bhmt* gene and defined a potentially sensitive region with mostly decreased methylation. Analyzing Hybrid Mouse Diversity Panel data, which consisted of 100 inbred strains of mice, we identified 97 DMCs that were affected by *Bhmt* genetic variation in the same region, with 7 overlapping those found in *Bhmt*-null mice ($P < 0.001$). At all time points, we found a hypomethylated region mapping to *Iqgap2* (IQ motif-containing GTPase activating protein 2) and *F2rl2* (proteinase-activated receptor-3), 2 genes that were also silenced and underexpressed, respectively.—Lupu, D. S., Orozco, L. D., Wang, Y., Cullen, J. M., Pellegrini, M., Zeisel, S. H. Altered methylation of specific DNA loci in the liver of *Bhmt*-null mice results in repression of *Iqgap2* and *F2rl2* and is associated with development of preneoplastic foci. FASEB J. 31, 2090–2103 (2017). www.fasebj.org

KEY WORDS: betaine · folate · epigenetics · methylome

Gene expression is regulated in liver, in part, *via* methylation of DNA (1) by using *S*-adenosylmethionine (AdoMet) as methyl donor (2, 3). AdoMet is formed in the liver by 2 alternative pathways, one that derives methyl groups from 5-methyl-tetrahydrofolate (5-MTHF) and one from betaine. The betaine pathway for AdoMet synthesis involves methylation of homocysteine (Hcy) to form methionine, a reaction catalyzed by betaine-homocysteine *S*-methyltransferase (BHMT). This enzyme generates approximately half of the methionine necessary for AdoMet synthesis (4). *S*-Adenosylhomocysteine (AdoHcy) is a competitive inhibitor of AdoMet-to-methyltransferases binding and, thus, the ratio of AdoMet to AdoHcy determines methyltransferase activity—also called methylation potential—within a cell (5).

A substantial body of research exists with regard to the contribution of the folate pathway to the epigenetic regulation of gene expression *via* DNA and histone methylation (6–9), and it is assumed that this pathway is rate limiting. Less is known about the impact of the betaine pathway on DNA methylation and gene expression. The BHMT pathway is important as 64% of *Bhmt* (betaine-homocysteine methyl transferase)-null mice develop hepatocellular carcinomas (HCCs) or hepatocellular adenomas at age 1 yr (10), and single-nucleotide

ABBREVIATIONS: 5-MTHF, 5-methyl-tetrahydrofolate; AdoHcy, *S*-adenosylhomocysteine; AdoMet, *S*-adenosylmethionine; *Bhmt*, betaine-homocysteine methyltransferase; CK 8-18, cytokeratin 8-18; DMC, differentially methylated CpG; DNMT, DNA methyltransferase; F2rl2, proteinase-activated receptor-3; FDR, false discovery rate; GST-P, glutathione *S*-transferase; HCC, hepatocellular carcinoma; Hcy, homocysteine; HMDP, Hybrid Mouse Diversity Panel; Iqgap2, IQ motif containing GTPase activating protein 2; RRBS, reduced representation bisulfite sequencing; SNP, single-nucleotide polymorphism; WT, wild-type

[1] Correspondence: University of North Carolina at Chapel Hill, 500 Laureate Way, Kannapolis, NC 28081, USA. E-mail: steven_zeisel@unc.edu

doi: 10.1096/fj.201601169R

This article includes supplemental data. Please visit *http://www.fasebj.org* to obtain this information.

0892-6638/17/0031-2090 © FASEB

polymorphisms (SNPs) in *BHMT* in humans increase the risk for various types of cancers (11). In addition, a transcription variant of exon 4 results in BHMT loss of function in human HCC (12), and down-regulation of BHMT serves as a marker of tumorigenesis in liver tissue biopsies (13). The aim of this study was to determine the impact of blocking the betaine pathway on liver methylation potential and the subsequent effect on DNA methylation, transcriptomic patterns, and phenotypic changes related to HCC development in this animal model.

For the first time, to our knowledge, we show that alterations in *Bhmt* result in accumulation of AdoHcy and betaine associated with epigenetic dysregulation at multiple genomic loci in mouse liver at 4 wk. These changes are correlated with altered gene expression in liver that are maintained from 4 to 52 wk. Finally, we observed loss of methylation for all time points in a region that was mapped to *Iqgap2* (IQ motif-containing GTPase activating protein 2) and *F2rl2* (proteinase-activated receptor-3)—repressed genes associated with hepatocellular carcinogenesis.

MATERIALS AND METHODS

Animal model and diets

C57BL/6J *Bhmt*-null mice were generated as previously described (10). Our mice were backcrossed to near congenicity (99.74%) so that C57Bl/6 wild-type (WT) mice could be used as suitable controls. Backcrossing was conducted by using marker-assisted accelerated backcrossing with a 384-mouse SNP panel (Charles River Laboratories, Northampton, MA, USA). C57BL/6J *Bhmt*-null and *Bhmt* WT mice were mated and maintained *ad libitum* on a modified AIN93G diet (with 1.4 g choline/kg for a total Met = 5.2 g/kg and total Cys = 3.9 g/kg; Dyets, Bethlehem, PA, USA); this diet meets mouse requirements for methionine, folate, and choline (14). The resulting heterozygous mice were mated by using a homozygous to homozygous breeding scheme while on the same diet, and the resulting pups were used for all experiments.

At 4, 12, 24, 52, and 78 wk, mice were anesthetized by using isoflurane and blood was collected by retro-orbital bleeding, and plasma was prepared and immediately stored at −80°C for later assessment of metabolites. Livers were collected and immediately freeze clamped with tongs that were cooled in liquid nitrogen and stored at −80°C until used to measure metabolites, DNA, and RNA, or were stored in 10% neutral buffered formalin. All procedures were performed according to protocols approved by the Animal Care and Use Committee of the National Institutes of Health (NIH; Bethesda, MD, USA).

Metabolic assessment

Concentrations of choline metabolites were measured by HPLC-electrospray ionization-isotope dilution mass spectrometry as previously described (15). Concentrations of AdoMet and AdoHcy were measured as previously described (16). Plasma total Hcy, cystathionine, and 5-MTHF were measured as previously described (17, 18). By using JMP Pro 12 (SAS Institute, Cary, NC, USA), data were checked for normality and equal variances and, where appropriate, the Student's *t* test or Welch's unequal variences *t* test was used.

Hematoxylin and eosin imaging, histologic scoring, glutathione *S*-transferase, and cytokeratin 8-18 staining and quantification

Fixed samples were processed routinely, embedded in paraffin, and sectioned at 6 uM. Sections were stained with hematoxylin and eosin. Slides were reviewed by a board-certified veterinary pathologist without prior knowledge of aminal status. Lesions were scored by using a subjective scale as follows: hepatic lipid accumulation; 1 = minimal; lipid vacuoles limited to the first 2 rows of hepatocytes surrounding the central vein; 2 = mild; lipid vacuoles involving up to 5 rows of hepatocytes surrounding the hepatic vein; 3 = moderate; lipid vacuoles that involved at least 5 rows of hepatocytes and distended hepatocyte outlines in at least 10% of hepatocytes; and 4 = marked; more than two thirds of hepatocytes in a lobule contained lipid vacuoles and approximately half or more of hepatocytes were distended. Neoplastic lesions were diagnosed by using the International Harmonization of Nomenclature and Diagnostic Criteria (INHAND) guidelines for proliferative and nonproliferative lesions of the rodent liver (19).

Immunohistochemical staining for placental glutathione *S*-transferase (GST-P) and cytokeratin 8-18 (CK 8-18) was performed according to manufacturer protocols (code no. 311; MBL, Nagoya, Japan; 20R-CP004; Fitzgerald, Acton, MA, USA) for paraffin-embedded sections. For GST-P, blocking was performed with normal horse serum followed by staining with ImmPress horseradish peroxidase anti-rabbit Ig (peroxidase) polymer detection kit and DAB Peroxidase substrate kit (Vector Labs, Burlingame, CA, USA). For CK 8-18, blocking was performed with goat serum followed by staining with Vectastain ABC-AP biotinylated anti-guinea pig Ig and ImmPact Vector Red Alkaline Phosphatase kit (Vector Labs). Total GST-P–positive areas and the number of CK 8-18–positive cells from random images were measured and counted with ImageJ (NIH, Bethesda, MD, USA).

Reduced representation bisulfite sequencing

DNA from liver (n = 8/group) was extracted by using the DNeasy Blood & Tissue Kit (Qiagen, Valencia, CA, USA) with a Qiacube robot (Qiagen). Reduced representation bisulfite sequencing (RRBS) was performed for 4-wk liver DNA as previously described (20) by Hudson Alpha Genomic Services Lab (Huntsville, AL, USA). Ovation RRBS methyl-seq system (NuGen, San Carlos, CA, USA) was used to generate the library, and the EpiTect Fast DNA Bisulfite Kit (Qiagen) was used for bisulfite conversion. The library quality and quantity was determined with a Qubit High Sensitivity (HS; Q32854; Thermo Fisher Scientific, Waltham, MA, USA) and an Agilent Bioanalyzer DNA 1000 kit (Agilent Technologies, Santa Cruz, CA, USA) followed by postprocessing Kapa RT-PCR (KK4873). This was followed by 50-bp single-end Illumina sequencing (Illumina HiSeq, v.4).

RRBS data analysis

Data that were generated by pyrosequencing were adapter-trimmed by using Trim Galore, v 0.3.7 (Babraham Bioinformatics, Cambridge, United Kingdom; *http://www.bioinformatics.babraham.ac.uk/projects/trim_galore/*), quality checked with FastQC (Babraham Bioinformatics; *http://www.bioinformatics.babraham.ac.uk/projects/fastqc/*), and mapped to the bisulfite converted mm9 genome using Bismark 0.12.3 (Baraham Bioinformatics; *http://www.bioinformatics.babraham.ac.uk/projects/bismark/*). CpGs with coverage grater than 10 reads that were present in all samples were analyzed by using a *t* test with estimated false discovery rate (FDR) of <5% using the

Storey method (21) and confirmed with the Avadis NGS data analysis platform (Strand Genomics, San Francisco, CA, USA). The resulting differentially methylated CpGs (DMCs) with δ methylation >10% were selected for further analysis. Noncoding DMCs were annotated to relevant genes by using the Genomic Regions Enrichment of Annotations Tool (GREAT) tool (22).

Pyrosequencing

Liver genomic DNA (500 ng) was treated with sodium bisulfite and purified (EpiTect Bisulfite Kit). The pyrosequencing assay was designed for the mus musculus *Iqgap2* gene by using PSQ 1.0 software (Qiagen) for a 281-base-pair sequence of interest that contained 7 CpG sites (starting at 96,549,324 in intron 1, chromosome 13, mm9). The biotinylated strand of amplified DNA was subjected to pyrosequencing on a PyroMark MD machine (Qiagen) as previously described (23), and values across all sites were averaged to express the average methylation across each sequence. Data analysis was performed with JMP Pro 12 using Student's *t* test with an adjusted α level for multiple comparisons equal to 0.007. Sequencing data are available in the ArrayExpress database (*http://www.ebi.ac.uk/arrayexpress*) under accession number E-MTAB-5204.

Gene expression arrays

RNA from liver (n = 8/group) was extracted by using the RNeasy Plus Universal Mini Kit (Qiagen) with a Qiacube robot, and the quality was checked by an Agilent 2100 Bioanalyzer (Agilent Technologies). The following products from Thermo Fisher Scientific were used: GeneChip ST Whole-Transcript Array 2.0 to measure mRNA and long intergenic noncoding RNA (lincRNA) at 4 and 52 wk; GeneChip WT Plus Reagent Kit to generate sense-strand cDNA from total RNA; and fragmented and labeled cDNA to prepare a hybridization cocktail with the GeneTitan Hybridization Wash and Stain Kit for WT arrays. Hybridization, washing, staining, and scanning of the Affymetrix (Thermo Fisher Scientific) peg plate arrays was carried out by using the GeneTitan MC Instrument. GeneChip Command Console Software was used for GeneTitan Instrument control.

Affymetrix Expression Console Software (Thermo Fisher Scientific) was used for basic data analysis and quality control. Gene-level differential expression analysis was performed by a 1-way between-subject ANOVA with multitesting correction performed by using Benjamini-Hochberg Step-Up FDR-controlling procedure (FDR < 0.05). Statistical analysis and visualization were done with the Affymetrix Transcriptome Analysis Console Software [Kyoto Encyclopedia of Genes and Genomes (KEGG) analysis was performed with WebGestalt using a hypergeometric test with Benjamini and Hochberg adjustment; *http://www.webgestalt.org*] (24). Microarray data are available in the ArrayExpress database (*http://www.ebi.ac.uk/arrayexpress*) under accession number E-MTAB-5203.

Copy number variation

Two independent assays were performed to determine genetic variation in the *Bhmt* geneby using Taqman Copy Number Assays (Thermo Fisher Scientific), ID Mm00387158_cn for an 81-bp amplicon overlapping intron 4–exon 5, and Mm00387159_cn corresponding to an 89-bp amplicon overlapping intron 5–exon 6, which is encompassed in the region excised in *Bhmt*-null mouse. Samples were run in quadruplicate according to manufacturer protocol, and each replicate was normalized to the transferrin receptor gene reference assay located on chromosome 16 and averaged for each sample, followed by a final normalization to a unique calibrator sample (WT C57Bl/6J mouse liver DNA). Data analysis was performed with Copy Caller, v.2.0 software (Applied Biosystems, Foster City, CA, USA).

RT-PCR gene expression

cDNA synthesis was performed by using a QuantiTect reverse transcription kit (Qiagen) on an Eppendorf Mastercycler ProS (Eppendorf, Hamburg, Germany). Amplification was performed by using the QuantiTect SYBR Green PCR kit (Qiagen). QuantiTect primer assays (Qiagen) were purchased for the following genes: *Iqgap2*, *F2rl2*, and *Eef2* (eukaryotic translation elongation factor 2; used as internal reference for each sample). Statistical analysis was carried out using JMP Pro 12 software.

Genome-wide association study

We tested for association between methylation levels as phenotypes and SNPs as predictors by using Efficient Mixed Model Algorithm (EMMA) to test for association and to account for population structure and relatedness among mouse strains, as previously described (25). We applied the model, $y = \mu + x\beta + u + e$, where μ is the mean, x is SNP, β is SNP effect, and u is the random effects as a result of relatedness, with $\mathrm{Var}(u) = \sigma_g^2 K$ and $\mathrm{Var}(e) = \sigma_e^2$, where K is identity-by-state matrix across all SNPs. We computed a restricted maximum likelihood estimate for $\sigma_g^2 K$ and σ_e^2, and we performed association on the basis of the estimated variance component with an F test to test that β does not equal 0.

Comparison of C57BL/6J with 129X1/SvJ

To test for differences in methylation at specific sites between C57BL/6J (B6) and 129X1/SvJ (129) mice, we used the binomial distribution with parameters P = percent methylation at that site, and n = total number of counts, and estimated 95% confidence intervals using *binofit* in MatLab (MathWorks, Natick, MA, USA), as previously described (26). Sites were considered differentially methylated between 2 samples if the mean methylation of each sample was outside of the 95% confidence interval of the other sample and if the difference between the mean methylation δ was >10%.

RESULTS

Bhmt deletion decreased methylation potential in liver, increased homocysteine concentrations, and altered related metabolites

We collected livers from 4, 12, 24, and 52-wk-old *Bhmt*-null and WT mice to measure metabolites of the transmethylation and choline oxidation pathways (**Fig. 1*A***). We first asked whether BHMT loss of function affects the methylation potential in liver. *Bhmt* deletion resulted in a 1.4-fold decrease in AdoMet ($P < 0.04$) only at 4 wk, with no significant difference at other time points (**Table 1**). Across all time points, there was a 2.3- to 4.2-fold increase

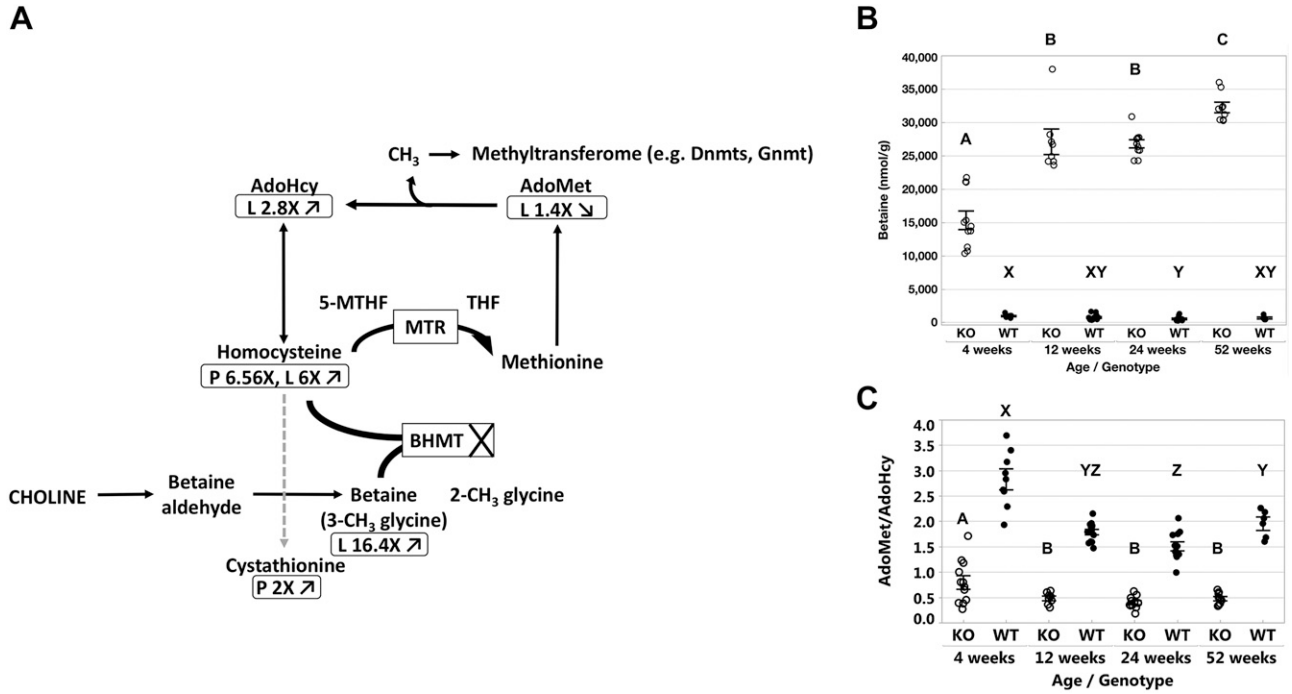

Figure 1. The folate- and betaine-dependent pathways generating *S*-adenosylmethionine in *Bhmt*-null and WT mice at 4 wk. *A*) One-carbon metabolite concentrations were measured by HPLC-electrospray ionization-isotope dilution mass spectrometry or by HPLC. Fold-changes [*Bhmt*-null (KO) /WT] in liver (L) and plasma (P) are indicated in boxes below the metabolite name ($P < 0.05$). *B*) Betaine concentration (nmol/g) in livers from 4-, 12-, 24-, and 52-wk-old KO and WT mice. *C*) Methylation potential (*S*-adenosylmethionin/*S*-adenosylhomocysteine) in livers from 4-, 12-, 24-, and 52-wk-old KO and WT mice; $n = 6$–8 per group. Different letters = $P < 0.05$ by Student's *t* test, with KO (A, B, C) and WT (X, Y, Z) comparison across time points. All comparisons between KO and WT are significant ($P < 0.05$); MTR, 5-methyl-tetrahydrofolate -homocysteine *S*-methyltransferase; THF, tetrahydrofolate; CH_3 – methyl group; Gnmt, glycine *N*-methyltransferase; ↗, increased; ↘, decreased.

in AdoHcy concentrations ($P < 0.001$; Table 1), with a 3.5- to 4.2-fold decrease in methylation potential (AdoMet/AdoHcy; $P < 0.0001$; Fig. 1C). We next investigated how blocking the betaine-dependent homocysteine remethylation alters the concentration of relevant metabolites in the alternative folate-dependent pathway and the choline oxidation and trans-sulfuration pathways. Liver betaine concentrations increased by 16.4- to 53-fold ($P < 0.0005$; Fig. 1B), homocysteine concentrations increased by 5- to 6.8-fold in liver ($P < 0.0005$) and 4.4- to 13.1-fold in plasma ($P < 0.0001$), and plasma cystathionine concentrations increased by 2- to 3.5-fold ($P < 0.0002$) in *Bhmt*-null mice (Fig. 1A and Table 1). There was no significant difference in plasma 5-MTHF concentrations between the 2 groups at 4 wk, with 1.6-fold-lower concentrations at both 12 and 52 wk ($P < 0.01$; Table 1). Additional data on betaine (choline oxidation) pathway metabolite concentrations can be found in Table 1. These data show that BHMT is important for maintaining a normal methylation potential and that the folate pathway is not sufficient to maintain low, normal concentrations of homocysteine across all time points.

Bhmt deletion results in morphologic changes and increased GST-P and CK 8-18 staining

We assessed the histologic profiles associated with *Bhmt* deletion at age 4, 12, 24, 52, and 78 wk. At 4 wk, 6 of 8 *Bhmt*-null mice had evidence of minimal or mild centrilobular lipid vacuolization of hepatocytes (**Fig. 2*B*** and Supplemental Table 1), with no evident abnormalities in WT mice (Fig. 2*A* and Supplemental Table 1). At 12 wk (Supplemental Fig. 1*A*, *B*) and 24 wk (Supplemental Fig. 1*C*, *D*), there were no significant changes other than minimal lipid vacuolization of centrilobular hepatocytes in *Bhmt*-null mice. At 52 wk, we observed preneoplastic lesions, foci of cellular alteration, and intrahepatic hemangiosarcoma (1 of 5) in *Bhmt*-null mice (Fig. 2*D* and Supplemental Table 1); there was mild ($n = 1$) and moderate ($n = 3$) to marked ($n = 1$) lipid vacuolization of hepatocytes in all 5 *Bhmt*-null mice (Supplemental Table 1). At 52 wk, there were no significant lesions in 4 of 5 WT mice, with one presenting minimal evidence of lipid vacuolization of hepatocytes (Fig. 2*C* and Supplemental Table 1). At 78 wk, overt hepatocellular adenomas and HCCs were evident in 2 of 2 of surviving *Bhmt*-null mice (Fig. 2*F*).

We examined the timing of initiation and proportion of liver expressing GST-P activity, a marker for preneoplastic foci (27), in *Bhmt*-null compared with WT liver. At 4 wk, there was no difference in GST-P staining (Fig. 2*G*, *H*), but starting with 12 and 24 wk, we observed a zonal distribution of increased GST-P activity in livers, with significant differences between *Bhmt*-null (Supplemental Fig. 1*F*, *H*) compared with WT (Supplemental Fig. 1*E*, *G*). At 52 wk, we continued to see 60% of liver area staining for GST-P–positive cells in *Bhmt*-null mice (Fig. 2*J*, *K*) compared with 30% of liver area staining for GST-P–positive cells in WT mice (Fig. 2*I*, *K*). Using another marker for

TABLE 1. *Concentration of metabolites of the transmethylation and choline oxidation pathways*

	Liver (nmol/g)								Plasma (μM)		
Metabolite	AdoMet	AdoHcy	Hcy	Choline	Glycerophospho-choline	Phosphocholine	Phosphatidylcholine	Sphingomyelin	5-MTHF	Hcy	Cystathionine
4 wk											
Bhmt-null	47 ± 6	64 ± 5	66 ± 8	68 ± 14	216 ± 22	71 ± 10	16,037 ± 1572	1168 ± 66	178 ± 15	54 ± 4	3998 ± 338
WT	65 ± 5	23 ± 2	11 ± 3	124 ± 32	485 ± 75	120 ± 16	16,027 ± 728	1088 ± 63	183 ± 1	8 ± 1	1970 ± 17
Fold change (null/WT)	−1.4*	2.8**	6**	−1.8	−2.2**	−1.7*	1	1.1	1	6.5**	2**
12 wk											
Bhmt-null	40 ± 2	87 ± 6	70 ± 2	87 ± 4	245 ± 9	136 ± 9	22,555 ± 1134	1304 ± 47	101 ± 5	54 ± 6	3175 ± 111
WT	53 ± 1.6	30 ± 0.6	10 ± 1	148 ± 24	1017 ± 111	203 ± 26	21,204 ± 717	1170 ± 47	159 ± 9	4 ± 1	908 ± 116
Fold change (null/WT)	−1.3	2.3*	6.85*	−1.7	−4.1**	−1.5*	1.06	1.1	−1.6**	13.1**	3.5**
24 wk											
Bhmt-null	37 ± 2	96 ± 6	NA	78.7 ± 10	229 ± 11	118 ± 11	22,281 ± 1026	1237 ± 31	NA	NA	NA
WT	35 ± 2.8	23 ± 1.2	NA	107 ± 23	868 ± 123	239 ± 48	19,463 ± 1022	1196 ± 62	NA	NA	NA
Fold change (null/WT)	1	4.2*	NA	−1.4	−3.8*	−2*	1.1	1	NA	NA	NA
52 wk											
Bhmt-null	38 ± 2	86 ± 6	68 ± 6	68 ± 6	251 ± 17	168 ± 17	21,085 ± 609	1270 ± 29	84 ± 7	69 ± 7	3460 ± 232
WT	41 ± 3	21 ± 0.4	14 ± 5	70 ± 7	605 ± 68	498 ± 76	19,078 ± 240	1023 ± 40	132 ± 10	16 ± 12	1501 ± 555
Fold change (null/WT)	−1.07	4.1*	5**	1	−2.4**	−2.9**	1.1	1.2**	−1.6**	4.4**	2.3**

Data are presented as mean ± SE, $n = 6$–8 per group. NA, not applicable. *$P < 0.05$, **$P < 0.01$ by Student's t test or Welch's unequal variances t test.

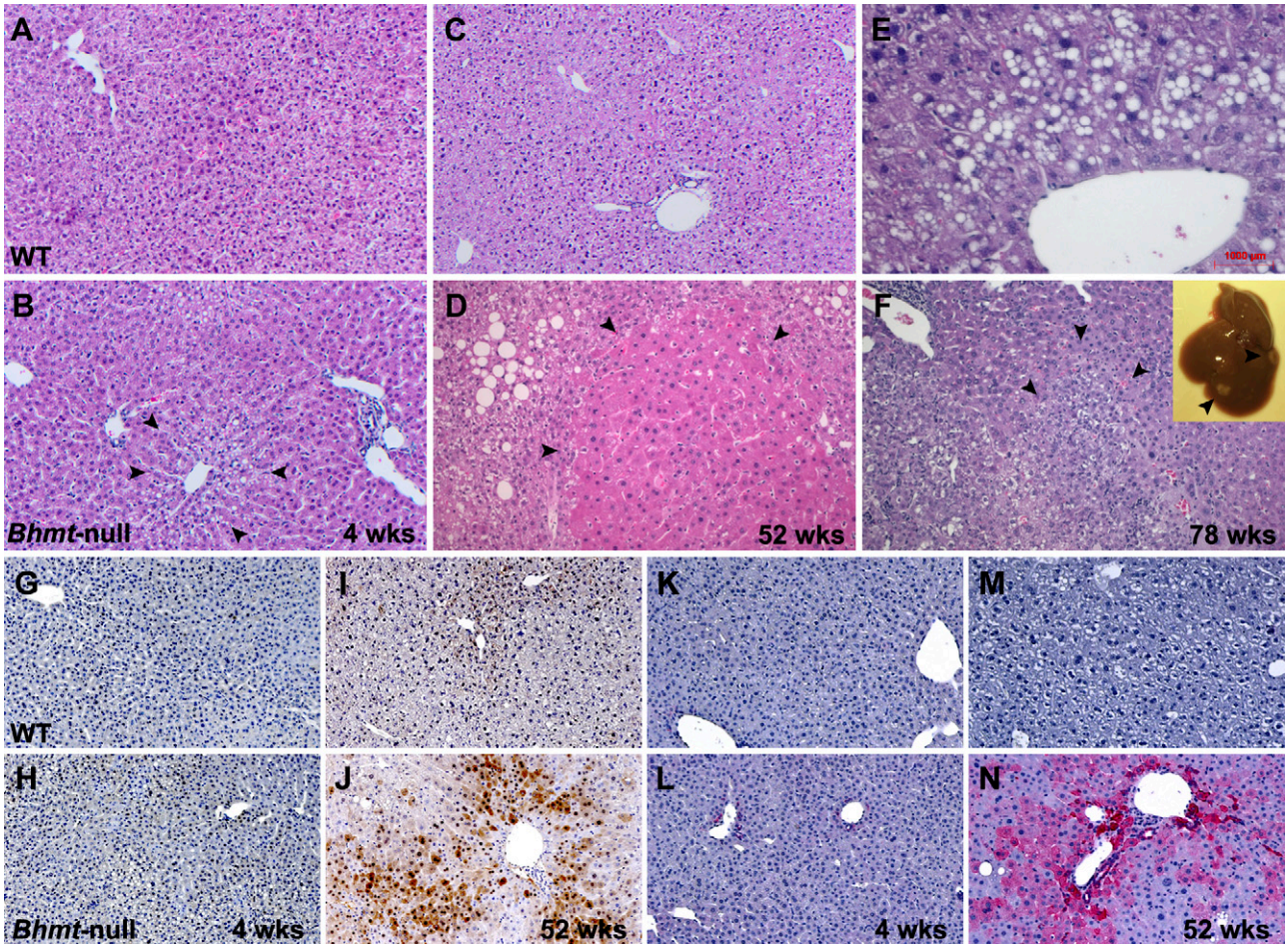

Figure 2. *Bhmt* deletion results in progressive changes in liver histology, including development of foci of increased GST-P and CK 8-18 expression in liver. Light microscopy of liver sections from 4-wk normal WT (*A*); *Bhmt*-null (KO) showing mild centrilobular vacuolization (arrowheads) (*B*); 52-wk normal WT (arrowheads) (*C*); 52-wk KO with preneoplastic focus (arrowheads) (*D*); 78-wk WT with lipid vacuolization (*E*); KO with hepatocellular carcinoma (arrowheads; inset: macroscopic nodules) (*F*); 4-wk WT and KO liver with no difference in GST-P activity (*G, H*); 52-wk WT with some increased GST-P activity (brown) (*I*) *vs.* 52-wk KO with significantly increased GST-P activity (*J*); 4-wk WT and KO liver with no difference in CK 8-18 staining (*K, L*); 52-wk WT with no increase in CK 8-18 staining (light red) (*M*) *vs.* 52-wk KO with significantly increased CK 8-18 staining (*N*). Magnification, ×20.

preneoplastic changes in liver, CK 8-18 (28), we confirmed that in *Bhmt*-null *vs*. WT liver, there were no differences at 4 wk, whereas there was a 23-fold increase in the number of CK 8-18–positive cells at 52 wk.

Identification of DMCs associated with loss of betaine use as a methyl donor in 4-wk liver

We next measured the effect of observed methylation potential decrease on liver DNA methylation patterns at 4 wk. We used RRBS to measure DNA methylation differences in livers of *Bhmt*-null and WT mice ($n = 8$/group). We filtered sequencing data for CpGs with at least 10× coverage and present in all samples, which left 1,188,488 CpGs available for analysis. BHMT loss of function did not cause widely distributed changes in DNA methylation in CpG-rich regions, with both groups presenting similar patterns of methylation (Supplemental Fig. 2), but rather, we observed that deleting *Bhmt* caused mostly loss of methylation at specific CpGs across the genome. We identified 63 DMCs (FDR < 5%) with a methylation difference of >10% between WT and KO groups, as previously described (21). Most of the DMCs have methylation differences much greater than 10%, with some reaching as much as 90–98%. These DMCs were distributed across 14 chromosomes, proximal to 81 genes (Supplemental Table 2). DMCs were mapped to proximal genes by using GREAT (22) with default settings (proximal 5 kb upstream and 1 kb downstream and distal up to 1000 kb). Clustering of samples and sites by using the euclidean distance metric grouped them according to genotypes, with 55 hypomethylated and 8 hypermethylated DMCs in *Bhmt*-null compared with WT mice (**Fig. 3*A***).

Identification of a differentially methylated genomic block on chromosome 13 at 4 wk

We observed that a total of 33 DMCs between *Bhmt*-null and WT mouse were located in 1 locus that spanned 15.5 Mb on chromosome 13 [from 93.5 to 109 Mb (mm9), which includes the *Bhmt* gene located at chromosome 13: 94,386,846–94,407,713; **Fig. 4*A***]. Of these 33 DMCs, 29 had

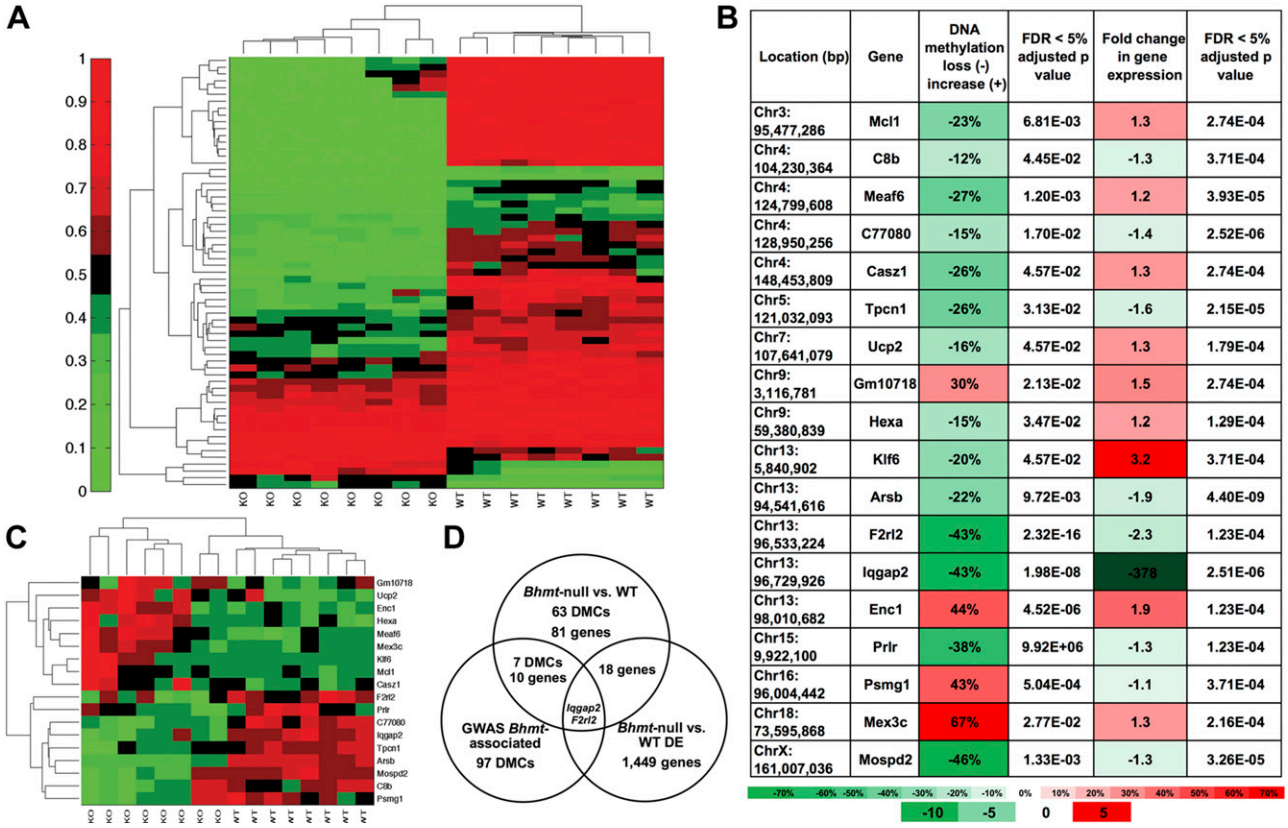

Location (bp)	Gene	DNA methylation loss (-) increase (+)	FDR < 5% adjusted p value	Fold change in gene expression	FDR < 5% adjusted p value
Chr3: 95,477,286	Mcl1	-23%	6.81E-03	1.3	2.74E-04
Chr4: 104,230,364	C8b	-12%	4.45E-02	-1.3	3.71E-04
Chr4: 124,799,608	Meaf6	-27%	1.20E-03	1.2	3.93E-05
Chr4: 128,950,256	C77080	-15%	1.70E-02	-1.4	2.52E-06
Chr4: 148,453,809	Casz1	-26%	4.57E-02	1.3	2.74E-04
Chr5: 121,032,093	Tpcn1	-26%	3.13E-02	-1.6	2.15E-05
Chr7: 107,641,079	Ucp2	-16%	4.57E-02	1.3	1.79E-04
Chr9: 3,116,781	Gm10718	30%	2.13E-02	1.5	2.74E-04
Chr9: 59,380,839	Hexa	-15%	3.47E-02	1.2	1.29E-04
Chr13: 5,840,902	Klf6	-20%	4.57E-02	3.2	3.71E-04
Chr13: 94,541,616	Arsb	-22%	9.72E-03	-1.9	4.40E-09
Chr13: 96,533,224	F2rl2	-43%	2.32E-16	-2.3	1.23E-04
Chr13: 96,729,926	Iqgap2	-43%	1.98E-08	-378	2.51E-06
Chr13: 98,010,682	Enc1	44%	4.52E-06	1.9	1.23E-04
Chr15: 9,922,100	Prlr	-38%	9.92E+06	-1.3	1.23E-04
Chr16: 96,004,442	Psmg1	43%	5.04E-04	-1.1	3.71E-04
Chr18: 73,595,868	Mex3c	67%	2.77E-02	1.3	2.16E-04
ChrX: 161,007,036	Mospd2	-46%	1.33E-03	-1.3	3.26E-05

Figure 3. DMCs and differentially expressed genes in *Bhmt*-null (KO) *vs.* WT liver. *A*) Clustergram by euclidean distance metric of methylation levels of statistically significant DMCs in the order of the genomic position (FDR < 5%) generated by RRBS in 4-wk liver; $n = 8$ per group, green to red represents 0–100% methylation. *B*) Genes with DMCs and differential gene expression (FDR < 5%). Green to red represents lower to higher methylation levels and lower to higher fold change of gene expression in KO *vs.* WT. *C*) Clustergram by euclidean distance metric of transcription levels of 18 statistically significant genes (FDR < 5%) with differential methylation in KO *vs.* WT. Green, lower expression; red, higher expression in the KO *vs.* WT. *D*) Venn diagram of DMCs and differentially expressed (DE) genes found in 4-wk livers of *Bhmt*-null *vs.* WT and in *Bhmt*-associated genome-wide association study DMCs.

lower methylation in *Bhmt*-null mouse, with differences ranging from −16 to −98%. We examined the CpG distribution in the genome and found that there was no bias toward chromosome 13, with only 4% of all CpGs located on that chromosome (Supplemental Fig. 3) compared with 52% of all DMCs found there (Supplemental Fig. 4).

Because *Bhmt* is located within the differentially methylated chromosome 13 locus, we checked whether, in *Bhmt*-null mouse (with exons 6 and 7 deleted), there were additional deletions introduced when generating the animal model. We assessed copy number variation using several probes: one that overlapped intron 5–exon 6, which showed no coverage in *Bhmt*-null mouse and 2 copies in *Bhmt* WT mouse (Supplemental Fig. 5); and one that overlapped intron 4–exon 5, showing 2 copies in both *Bhmt*-null and *Bhmt* WT mice (Supplemental Fig. 6). We also verified that the observed methylation differences were not a result of genetic variants between *Bhmt*-null and WT. *Bhmt*-null allele was originally generated in the 129X1/SvJ mouse strain and backcrossed to the C57BL/6J strain; however, it is possible that some vestige of the original 129X1/SvJ strain DNA near the *Bhmt* locus remained, and that methylation differences between C57BL/6J and 129X1/SvJ strains could explain the differences observed on chromosome 13. To examine this possibility, we compared methylation levels between the 129X1/SvJ and C57BL6J strains and looked at cytosines with differential methylation levels >10% between the 2 strains, as previously described (26). We found only 7 DMCs of 63 were differentially methylated between the 2 strains, with overall no significant enrichment in differentially methylated sites in the chromosome 13 locus relative to the rest of the chromosome ($P = 0.27$; Supplemental Fig. 7). These results suggest that *Bhmt*-null mouse has a mostly hypomethylated region on chromosome 13 in 4-wk liver, which is sensitive to the decreased methylation potential.

Identification of liver transcriptomic changes in *Bhmt*-null mouse

We asked whether there were any expression changes in liver genes that are associated with loss of BHMT function and how they relate across time. We computed the robust multichip average normalized expression of 34,472 genes that were available for analysis and found that 1449 (4.2%) and 1513 (4.3%) were significantly

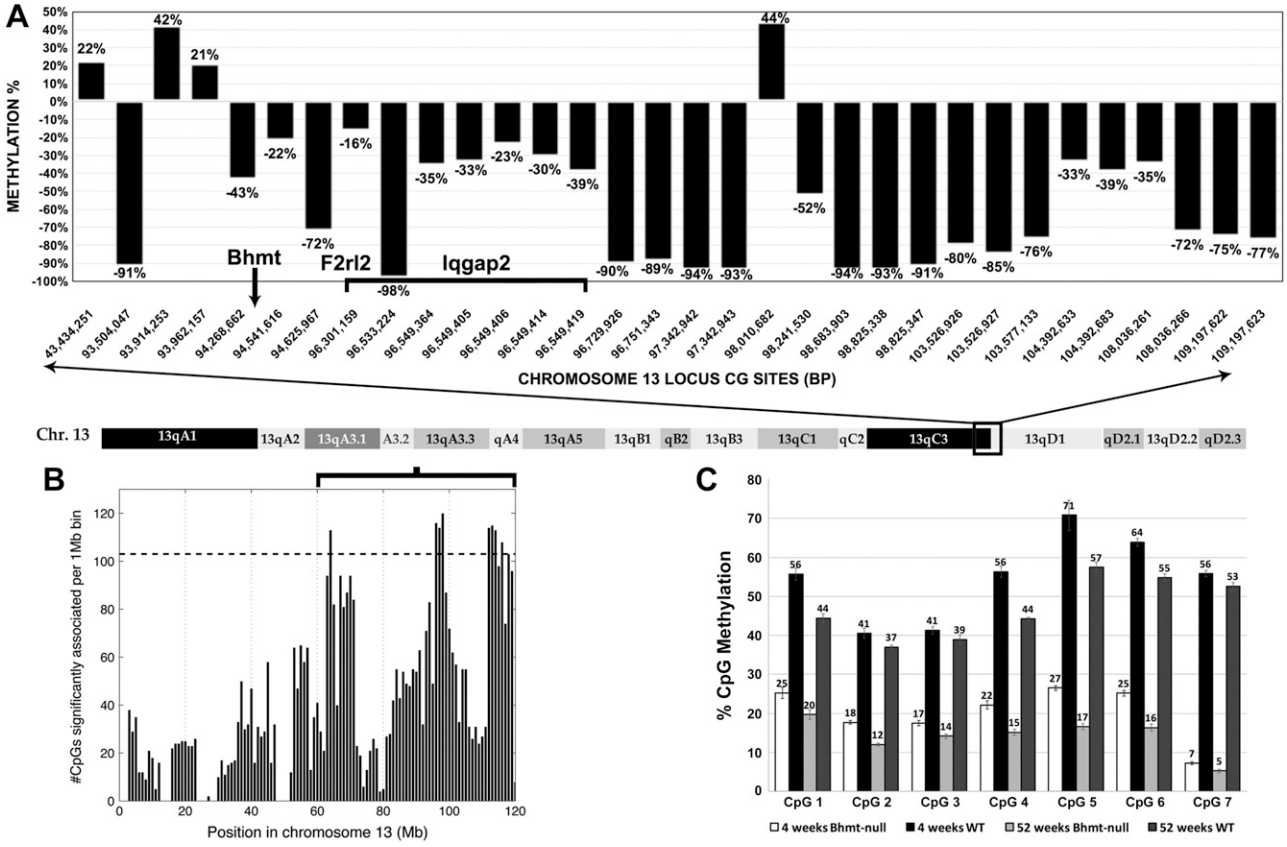

Figure 4. Hypomethylated block on chromosome 13 (Chr. 13), also confirmed by genome-wide association study (GWAS). *A*) Graph of DMCs in a locus spanning 15 Mb in chromosome 13, generated from RRBS in 4-wk livers. *X* axis, genomic position (bp) of DMCs in chromosome 13 (distance between data points not proportional); *y* axis, percentage δ-methylation gain (positive values) or loss (negative values) for *Bhmt*-null (KO) *vs.* WT. Arrow shows approximate location for the *Bhmt* gene; bracket shows approximate location of the *F2rl2* and *Iqgap2* genes relative to DMCs. *B*) GWAS analysis using the Hybrid Mouse Diversity Panel data, testing for associations between SNPs found at the *Bhmt* locus (as predictors) and DNA methylation (as phenotypes) within 10 Mb of the *Bhmt* genomic bin. *Y* axis, number of CpGs mapping to each 1 Mb; *x* axis, chromosome 13 position of each bin. The horizontal dotted line is the Poisson significance threshold for each hotspot bin. Bracket represents the hotspot of CpGs associated with genetic variation in *Bhmt*. *C*) Pyrosequencing of chromosome13 locus sampling of 7 consecutive CpGs in an area mapping to *Iqgap2* and *F2rl2* genes. *X* axis, 7 consecutive DMCs found in intron 2 of the *Iqgap2* gene; *y* axis, percent CpG absolute methylation; white bars, 4-wk KO; black bars, 4-wk WT; light gray bars, 52-wk KO; dark gray bars, 52-wk WT.

(FDR < 5%) differentially expressed across the genome between *Bhmt*-null and WT mice (Supplemental Tables 3 and 4) at 4 and 52 wk, respectively. Of genes, 157 and 315 at 4 and 52 wk, respectively, had >2-fold differential expression difference in *Bhmt*-null *vs*. WT (**Fig. 5*D*, *F***). Main network functions associated with these transcriptomic changes that were consistent at both 4 and 52 wk were represented by liver molecular transport, lipid metabolism, and liver pathology (Fig. 5*A*–*C*). KEGG pathway enrichment analysis found glycine, serine, and threonine metabolism were the top 3 modified pathways (ratio of enrichment, 29.44; adjusted $P <$ 1.66E-05), with all genes presenting the same direction of change at 4 and 52 wk (Supplemental Table 5). There were expected common canonical pathway themes perturbed by deletion of *Bhmt*, such as AdoMet biosynthesis and methionine and homocysteine degradation, but also retinoid X receptor pathway activation at 4 wk ($P <$ 2.39E-04 with 21% overlap) and inhibition of retinoid X receptor function at 52 wk ($P <$ 2.84E-03 with 18.2% overlap). In a comparison analysis of upstream regulators, we found pregnane X receptor *Nr1I2* and *Trim24* (transcription regulator tripartite motif containing 24) to be activated ($P <$ 3.74E-04; *z* score, 2.8) and upstream regulators at both 4 and 52 wk to be inhibited ($P <$ 1.66E-03; *z* score, −2.2; Fig. 5*E*).

We asked whether expression levels were altered in the 81 genes proximal to DMCs at 4 wk. Of these 81 genes, 63 were represented in the Affymetrix array, and 18 were differentially expressed, clustering by transcription levels to genotype (P = 7.13E-12; Fig. 3*C*), with 9 up-regulated and 9 down-regulated (Fig. 3*B*). Of these, 6 were also differentially expressed at 52 wk (5 in the same direction, including *Iqgap2* and *F2rl2*). To validate the gene expression array, we performed RT-PCR for a group of 11 genes (data not shown). All results were in concordance with the microarray, including expression of *Iqgap2* (378- and 430-fold decrease in *Bhmt*-null) and *F2rl2* (2.3- and 3.3-fold decrease in *Bhmt*-null) at both 4 and 52 wk. These results confirm the

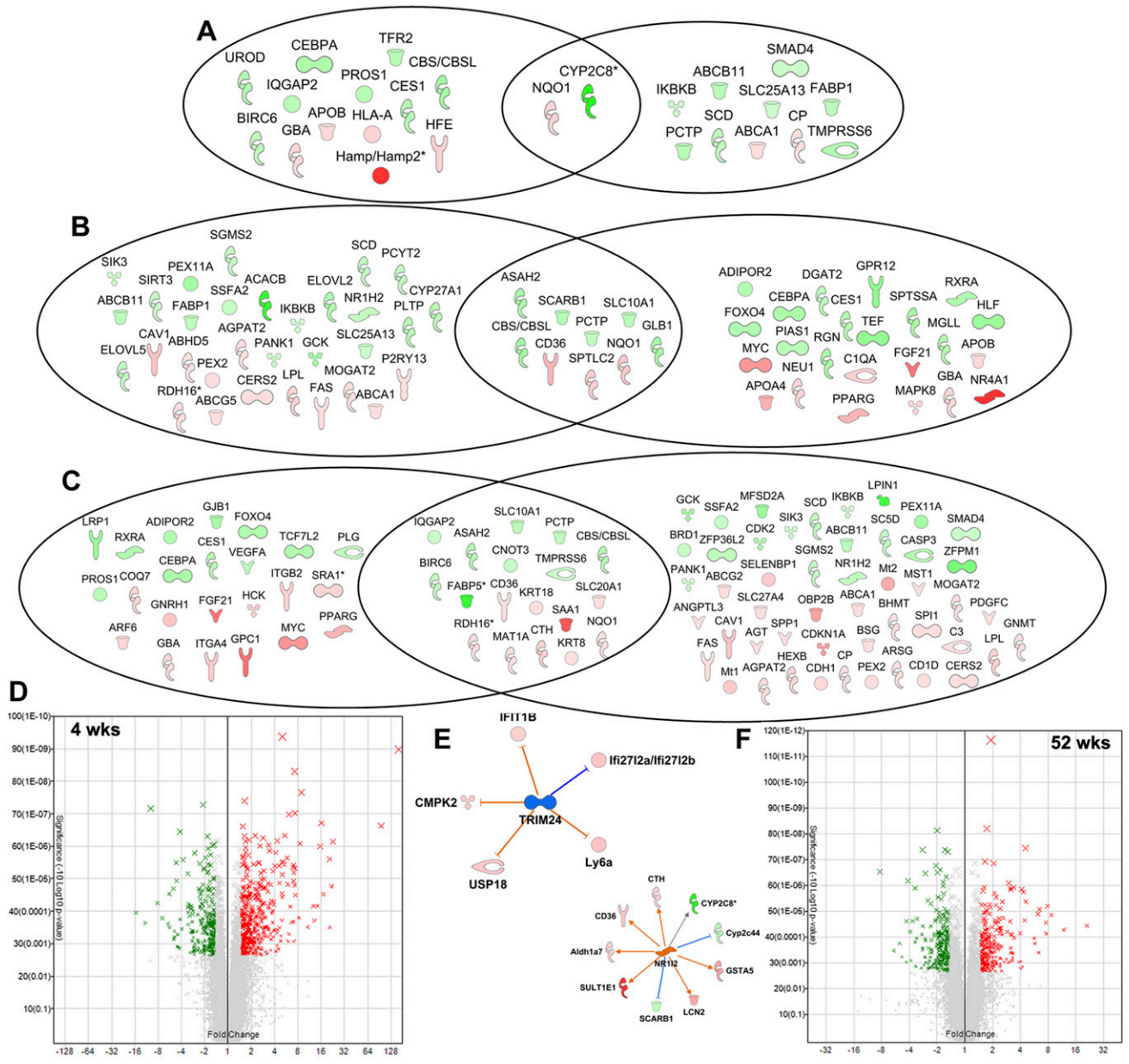

Figure 5. Differential gene expression at 4 and 52 wk in mouse liver. *A–C*) The main network functions associated with transcriptomic changes that were consistent at both 4 and 52 wk were represented by liver molecular transport (*A*), lipid metabolism (*B*), and liver pathology (*C*). *D*) Volcano plot of differentially expressed genes in liver at 4 wk (fold change ≤ -2 and ≥ 2). *E*) Nuclear receptor subfamily 1 group member 2 (*NR1I2*) and tripartite motif containing 24 (*Trim24*) are activated ($P < 3.74\text{E-}04$) and inhibited ($P < 1.66\text{E-}03$) upstream regulators at 4 and 52 wk, respectively. *F*) Volcano plot of differentially expressed genes in liver at 52 wk (fold change ≤ -2 and ≥ 2). Color intensity proportional with the fold change. Molecules found in intersecting ovals are common across both time points. Red, overexpressed; green, underexpressed.

perturbation of 1-carbon metabolism pathways and reveal multiple affected pathways that are relevant for normal liver function and development of HCC.

Genetic variation in *Bhmt* affects CpG methylation across the genome, especially on chromosome 13

By using another mouse population, we investigated whether genetic variation in the *Bhmt* gene was associated with DMCs across the genome, especially within chromosome 13. Using the Hybrid Mouse Diversity Panel (HMDP) RRBS liver data generated from 16-wk-old mice from 100 commercially available inbred strains (26), we applied a linear mixed model to test for associations between 79 SNPs that were found at the *Bhmt* locus (as predictors) and liver DNA methylation at individual CpG sites across the genome (as phenotypes). Significant association was set at the Bonferroni threshold with $P < 1.4\text{E-}12$. We found that 1958 DMCs were regulated by *Bhmt* genotypes, with 1827 located in chromosome 13, of which 1382 were in the

differentially methylated genomic block. We specifically asked whether DNA methylation near the *Bhmt* locus was associated with genetic variation at the *Bhmt* locus (*i.e.*, SNPs regulating DNA methylation levels in *cis*). To do so, we looked for CpGs within 10 Mb of *Bhmt* whose DNA methylation was associated with SNP variants in the 1-Mb locus surrounding the *Bhmt* start site. We chose these thresholds on the basis of linkage disequilibrium patterns in the HMDP population and on our prior observation that CpG methylation associations can exhibit long-range linkage disequilibrium (29). We found 97 unique CpGs to be influenced by SNPs at the *Bhmt* locus (Fig. 4*B*). These results suggest the existence of a larger region in chromosome 13 where DNA methylation is affected by genetic variation at the *Bhmt* locus.

Differentially methylated genes linked to *Bhmt* genetic variation

We wanted to determine whether there was any overlap between CpGs identified by the HMDP genome-wide association study and CpGs identified by RRBS analysis in *Bhmt*-null mice. We found 7 common DMCs ($P < 0.001$) that mapped to the following 10 genes by GREAT: *Thbs4* (thrombospondin 4), *Serinc5* (serine incorporator 5), *Papd4* (PAP-associated domain containing 4), *Lhfpl2*, *Arsb* (arylsulfatase B), *F2rl2*, *Iqgap2*, *Sv2c* (synaptic vesicle glycoprotein 2C), *Col4a3bp* [collagen type IV, alpha 3 (Goodpasture antigen) binding protein], and *Hmgcr* (3-hydroxy-3-methylglutaryl-CoA reductase). Two genes that were common between the 2 data sets—*Iqgap2*, located at chromosome 13: 96,397,132-96,661,877; and *F2rl2* located at chromosome 13: 96,466,875-96,472,723 (mm9)—were associated with a hypomethylated region identified by 7 CpGs. To validate these results, we performed pyrosequencing of a 281-bp amplicon that contained 3 DMCs (chromosome 13: 96,549,405–96,549,419, mm9) identified by RRBS and 4 additional CpGs that were found in intron 2 of the *Iqgap2* gene. All CpGs had significantly lower methylation in *Bhmt*-null mice (Tukey HSD, $P < 0.01$), ranging from 23 to 49%, which confirmed the results of the epigenome-wide DNA methylation screen (Fig. 4*C*). Methylation loss was preserved across time, from 4 to 52 wk (Fig. 4*C*).

DISCUSSION

Methylation reactions in the liver are dependent on the ratio of concentrations of AdoMet to AdoHcy (5). We show, for the first time to our knowledge, that betaine-dependent methylation of homocysteine (by BHMT) is important for maintaining AdoMet/AdoHcy in the liver and for maintaining normal patterns of DNA methylation. When BHMT function is lost, AdoHcy increases and AdoMet decreases. This decrease is associated with altered DNA methylation at specific CpG sites, with associated changes in gene expression and neoplastic changes in the liver.

GST-P and CK 8-18 are well-known markers of preneoplastic foci of cellular alteration in mouse and rat liver, and their expression is associated with an increased risk of HCC formation (28, 30–34). Together with the accumulation of betaine, Hcy, and AdoHcy in liver across time, we found liver morphologic changes and zonal increases in GST-P activity and CK 8-18 expression in *Bhmt*-null mice. These changes are consistent with the expansion of premalignant clones of abnormal hepatocytes in liver, a phenotype that evolves to hepatocellular adenomas and HCCs in *Bhmt*-null mouse.

We found that the BHMT pathway was essential for maintaining normal AdoMet/AdoHcy concentrations. Increased AdoHcy resulted in significantly decreased (from 3.5-fold at 4 wk to 4.2-fold at 52 wk) methylation potential (defined as the ratio of AdoMet to AdoHcy). A decrease in methylation potential of this magnitude reduces maximal DNA methyltransferase (DNMT) activity to 23% of control (35). AdoHcy has high affinity for DNMTs and competes for binding of AdoMet, thereby inhibiting DNMT enzymatic activity (36).

By using RRBS, we did not observe widely distributed DNA methylation changes in CpG-rich regions, but in *Bhmt*-null mouse livers, we found 63 DMCs proximal to 81 genes (Supplemental Table 2) in 14 chromosomes. The majority of those CpGs (87%) have an average 44% loss of methylation, with the rest gaining methylation status. Previous studies showed that feeding methyl-deficient diets was associated with both hypo- and hypermethylation of DNA (37, 38), with one potential mechanism being the up-regulation of active ten-eleven translocation DNA demethylation enzymes observed with methionine choline–deficient diets (39).

More than 50% of all highly statistically significant (FDR < 5%) DMCs were located on chromosome 13 in a 15.5-Mb locus, with predominantly loss of methylation. When we increased FDR to <10%, the locus was still over-represented with 38% of DMCs. The significance of long-range DNA methylation changes is not clear, with hypomethylated blocks ranging from 5 kb to 10 Mb being previously reported in colon samples, which differentiates normal tissue from colorectal cancer (40). These corresponded to large euchromatic and heterochromatic domains, such as lamina-associated domains and large organized chromatin lysine modifications (41). Altering these functional genomic regions can change proximity to the nuclear lamina, chromatin density, and DNA accessibility (40).

It is possible that the sensitivity to DNA methylation perturbations that we observed in chromosome 13 is a regulatory mechanism meant to sense methyl metabolism, as not only *Bhmt* but other 1-carbon metabolism genes are located there: *Dmgdh* (dimethylglycine dehydrogenase) at chromosome 13: 94,444,391; *Mtrr* (methionine synthase reductase) at chromosome 13: 68,699,657; and *Mtr* (5-methyltetrahydrofolate-homocysteine methyltransferase; also in chromosome 13 but outside the locus at 12,279,086).

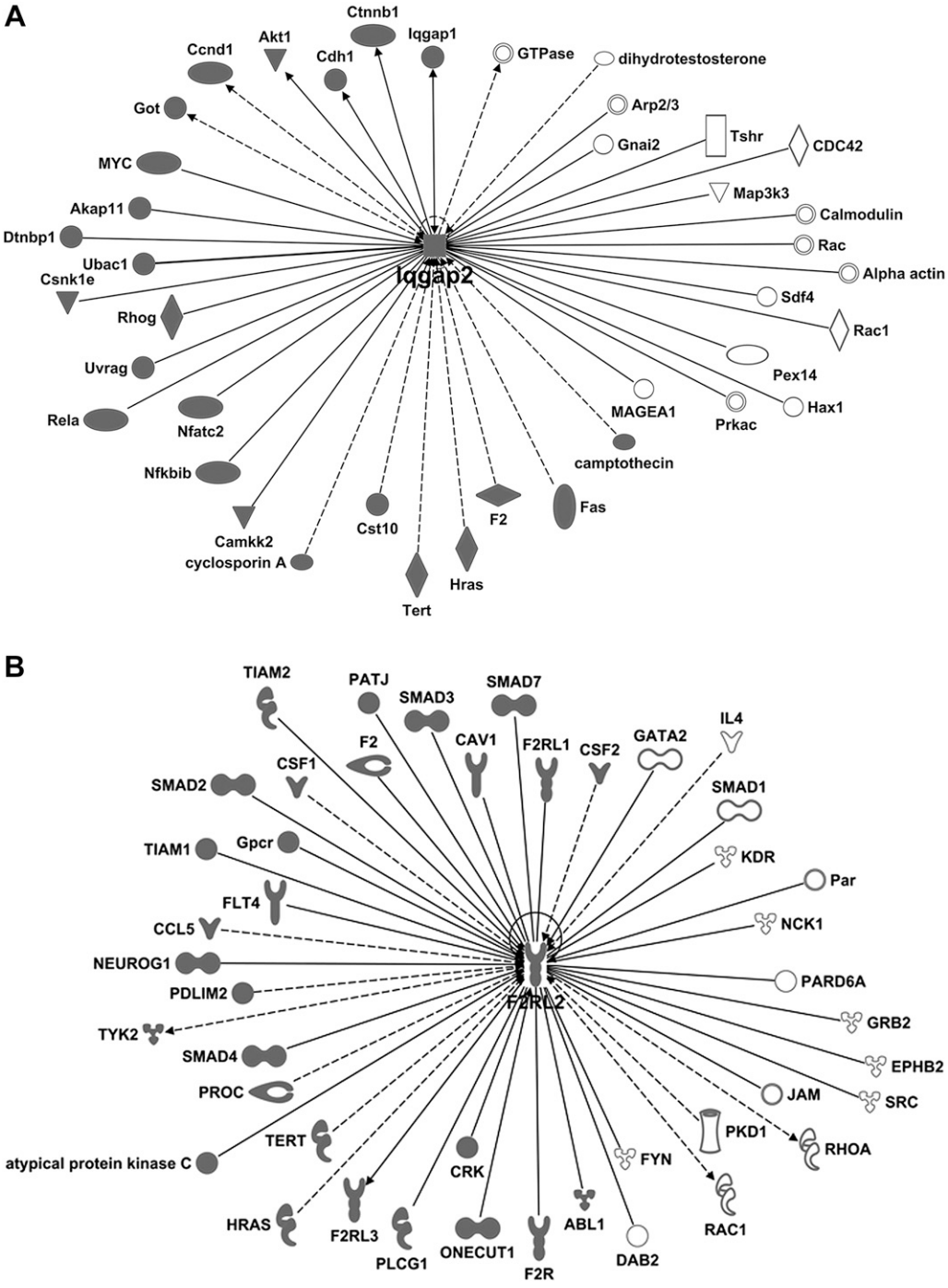

Figure 6. Ingenuity Pathway Analysis molecules interacting with *Iqgap2* (*A*) and *F2rl2* (*B*). Dark circles represent cancer-related interactions. Arrows show directionality of the effect, with solid and dotted arrows indicating direct or indirect relationship, respectively.

Altered DNA methylome in *Bhmt*-null mice is associated with changes in gene expression in the liver at 4 wk. Of the 18 highly significant (FDR $< 5\%$) differentially expressed genes (Table 1), 5 are located on chromosome 13, with 4 of the 5 falling within the chromosome 13 hypomethylated block: *Arsb, F2rl2, Iqgap2,* and *Enc1* (ectodermal-neural cortex 1). We performed an Ingenuity Pathway Analysis hepatotoxicity functional ranking and found that 7 of these genes were involved in liver hyperplasia/hyperproliferation, HCC, and liver necrosis/cell death. This suggests that DNA methylation and transcription changes occur early (4 wk) and before development of preneoplastic foci and HCC in *Bhmt*-null mouse, and that some of these changes are maintained through 52 wk of age (intersecting ovals in Fig. 5*A–C*, *E*).

Because gene deletions are not common in humans, but SNPs in *Bhmt* are, it is important that we observed that genetic polymorphisms in *Bhmt* that occur in different strains of mice also affected CpG methylation in *cis*. When

we overlap the results of the 2 study approaches, 7 DMCs are identified as highly significant by both methods. From the 10 genes that mapped to these sites, 2 genes, *Iqgap2* and *F2rl2*, with an average of 43% loss of methylation, are also underexpressed in *Bhmt*-null mouse liver across all time points (Figs. 3*B*, *D* and 5).

Iqgap2 and *F2rl2*—mapped to a hypomethylated region—were >378- and 5-fold underexpressed ($P < 0.01$), respectively, across all 4 time points. *Iqgap2* belongs to a family of scaffolding proteins, which mediate Rho GTPase and Ca^{2+}/calmodulin signaling in regulating multiple cellular processes, such as cell adhesion, motility, and exocytosis (42). *Iqgap2* silencing has metabolic effects, such as increasing mitochondrial methyl-donor metabolism by elevating *Gnmt* (Glycine *N*-methyltransferase) expression, the enzyme responsible for converting AdoMet to AdoHcy (43). *Iqgap2* is important in multiple reactions in the liver, regulating activation and translocation of β-catenin and expression of E-cadherin, as well as reacting to key regulators of liver neoplastic transformation, such as *c-Myc* (v-Myc avian myelocytomatosis viral oncogene homolog; **Fig. 6*A***) (44, 45). *F2rl2* is a member of the protease-activated receptor-3 family and is involved in homeostasis, adhesion, proliferation, and migration (Fig. 6*B*) (46, 47). Although we observed that both genes were hypomethylated at this specific site, we noticed a 76-fold difference in the extent of underexpression, with *Iqgap2* >378- and *F2rl2* >5-fold underexpressed. We suggest that the difference in gene expression between *Iqgap2* and *F2rl2* at this magnitude could be a result of methylation changes in different areas that bind transcription factors and separately control these genes. In addition, our region of interest in the body of the *Iqgap2* gene is enriched in histone 3 monomethyl Lys4, a marker of active enhancers that is a chromatin signature of DNA hypomethylation in stem and differentiated cells during aging (48). This could explain the sustained loss of methylation across time and why *Iqgap2* is silenced but *F2rl2* is only repressed.

The suppression of these 2 genes may explain why preneoplastic hepatic foci developed as early as 12 wk of age; the *Iqgap2*-null mice develop spontaneous HCCs (49), as do *Bhmt*-null mice (10), between 52 and 78 wk. Carcinogenesis is a process in which changes in gene expression result in cell clones that have lost some of the regulation that normally controls cell growth and proliferation (premalignant cells). When these cells develop further loss of regulatory mechanisms (the so-called second hit), they transform into frank carcinomas. We suggest that this is why we observe abnormal DNA methylation with perturbed expression of *Iqgap2* and *F2rl2* months before we observe development of carcinomas. *F2rl2* binds to signal transduction proteins and transcription factors that are involved in carcinogenesis (50, 51). These observations suggest that *Iqgap2* and *F2rl2* might be important players in coordinating genes that are responsible for normal liver function, and they are responsive to changes in 1-carbon metabolism, including genetic variation in *Bhmt*. We suggest that the observed reductions in expression of *Iqgap2* and *F2rl2* mediate hepatocarcinogenesis in *Bhmt*-null mice.

There are other mediators of HCC initiation associated with the *Bhmt*-null mouse model. One of the upstream regulators that controls multiple genes at both 4 and 52 wk in liver is *Trim24* (Fig. 5*E*), a tumor suppressor in mice, with gene deletion triggering hepatic injury, fibrosis, and HCC (52) *via* a retinoic-activated receptor–mediated mechanism (53).

For the first time to our knowledge, we show that silencing of *Bhmt*, one of the 2 key controllers of methyl flux metabolism, is associated with DNA methylation dysregulation, culminating in transcriptomic changes in the liver. In our study, we find that one region that mapped to *Iqgap2* and *F2rl2* genes is hypomethylated and associated with underexpression of both genes from age 4 wk—long before HCC develops in *Bhmt*-null mice—to 52 wk. Considering the potential impact of *Iqgap2* and *F2rl2* in HCC initiation and progression, future studies that address their response to *Bhmt* and 1-carbon metabolism changes in humans are needed. FJ

ACKNOWLEDGMENTS

This work was funded by the University of North Carolina Nutrition Research Institute and by a U.S. National Institutes of Health, National Institute of Diabetes and Digestive and Kidney Diseases Grant DK56350. The authors thank Jennifer Owen, for assisting with blinded analysis of GST-P–positive cells in liver, and Scott Jaworski, for help with figure editing (both from University of North Carolina at Chapel Hill).

AUTHOR CONTRIBUTIONS

D. S. Lupu drafted the manuscript, assisted in study design, generated samples, and generated and analyzed the data; L. D. Orozco assisted in study design and analyzed the data; Y. Wang generated and analyzed metabolic data; J. M. Cullen performed the histological analysis for liver samples; M. Pellegini assisted in study design and interpreted the data; S. H. Zeisel conceived the study, interpreted the data, and rewrote and finalized the manuscript; and all authors assisted in writing the manuscript and approved submission.

REFERENCES

1. Moore, L. D., Le, T., and Fan, G. (2013) DNA methylation and its basic function. *Neuropsychopharmacology* **38**, 23–38
2. Avila, M. A., García-Trevijano, E. R., Martínez-Chantar, M. L., Latasa, M. U., Pérez-Mato, I., Martínez-Cruz, L. A., del Pino, M. M., Corrales, F. J., and Mato, J. M. (2002) S-Adenosylmethionine revisited: its essential role in the regulation of liver function. *Alcohol* **27**, 163–167
3. Petrossian, T. C., and Clarke, S. G. (2011) Uncovering the human methyltransferasome. *Mol. Cell. Proteomics* **10**, 000976
4. Finkelstein, J. D., and Martin, J. J. (1984) Methionine metabolism in mammals. Distribution of homocysteine between competing pathways. *J. Biol. Chem.* **259**, 9508–9513
5. Tehlivets, O., Malanovic, N., Visram, M., Pavkov-Keller, T., and Keller, W. (2013) S-Adenosyl-L-homocysteine hydrolase and methylation disorders: yeast as a model system. *Biochim. Biophys. Acta* **1832**, 204–215
6. Salbaum, J. M., and Kappen, C. (2012) Genetic and epigenomic footprints of folate. *Prog. Mol. Biol. Transl. Sci.* **108**, 129–158

7. Kok, D. E., Dhonukshe-Rutten, R. A., Lute, C., Heil, S. G., Uitterlinden, A. G., van der Velde, N., van Meurs, J. B., van Schoor, N. M., Hooiveld, G. J., de Groot, L. C., Kampman, E., and Steegenga, W. T. (2015) The effects of long-term daily folic acid and vitamin B_{12} supplementation on genome-wide DNA methylation in elderly subjects. *Clin. Epigenetics* **7**, 121
8. Nilsson, E., Matte, A., Perfilyev, A., de Mello, V. D., Käkelä, P., Pihlajamäki, J., and Ling, C. (2015) Epigenetic alterations in human liver from subjects with type 2 diabetes in parallel with reduced folate levels. *J. Clin. Endocrinol. Metab.* **100**, E1491–E1501
9. Ly, A., Hoyt, L., Crowell, J., and Kim, Y. I. (2012) Folate and DNA methylation. *Antioxid. Redox Signal.* **17**, 302–326
10. Teng, Y. W., Mehedint, M. G., Garrow, T. A., and Zeisel, S. H. (2011) Deletion of betaine-homocysteine S-methyltransferase in mice perturbs choline and 1-carbon metabolism, resulting in fatty liver and hepatocellular carcinomas. *J. Biol. Chem.* **286**, 36258–36267
11. Koushik, A., Kraft, P., Fuchs, C. S., Hankinson, S. E., Willett, W. C., Giovannucci, E. L., and Hunter, D. J. (2006) Nonsynonymous polymorphisms in genes in the one-carbon metabolism pathway and associations with colorectal cancer. *Cancer Epidemiol. Biomarkers Prev.* **15**, 2408–2417
12. Pellanda, H., Namour, F., Fofou-Caillierez, M., Bressenot, A., Alberto, J. M., Chéry, C., Ayav, A., Bronowicki, J. P., Guéant, J. L., and Forges, T. (2012) A splicing variant leads to complete loss of function of betaine-homocysteine methyltransferase (BHMT) gene in hepatocellular carcinoma. *Int. J. Biochem. Cell Biol.* **44**, 385–392
13. Megger, D. A., Bracht, T., Kohl, M., Ahrens, M., Naboulsi, W., Weber, F., Hoffmann, A. C., Stephan, C., Kuhlmann, K., Eisenacher, M., Schlaak, J. F., Baba, H. A., Meyer, H. E., and Sitek, B. (2013) Proteomic differences between hepatocellular carcinoma and nontumorous liver tissue investigated by a combined gel-based and label-free quantitative proteomics study. *Mol. Cell. Proteomics* **12**, 2006–2020
14. National Research Council. (1995) *Nutrient Requirements of Laboratory Animals*, 4th revised ed., National Academies Press, Washington, D.C.
15. Koc, H., Mar, M. H., Ranasinghe, A., Swenberg, J. A., and Zeisel, S. H. (2002) Quantitation of choline and its metabolites in tissues and foods by liquid chromatography/electrospray ionization-isotope dilution mass spectrometry. *Anal. Chem.* **74**, 4734–4740
16. Molloy, A. M., Weir, D. G., Kennedy, G., Kennedy, S., and Scott, J. M. (1990) A new high performance liquid chromatographic method for the simultaneous measurement of S-adenosylmethionine and S-adenosylhomocysteine. Concentrations in pig tissues after inactivation of methionine synthase by nitrous oxide. *Biomed. Chromatogr.* **4**, 257–260
17. Ducros, V., Belva-Besnet, H., Casetta, B., and Favier, A. (2006) A robust liquid chromatography tandem mass spectrometry method for total plasma homocysteine determination in clinical practice. *Clin. Chem. Lab. Med.* **44**, 987–990
18. Saw, S. M., Yuan, J. M., Ong, C. N., Arakawa, K., Lee, H. P., Coetzee, G. A., and Yu, M. C. (2001) Genetic, dietary, and other lifestyle determinants of plasma homocysteine concentrations in middle-aged and older Chinese men and women in Singapore. *Am. J. Clin. Nutr.* **73**, 232–239
19. Thoolen, B., Maronpot, R. R., Harada, T., Nyska, A., Rousseaux, C., Nolte, T., Malarkey, D. E., Kaufmann, W., Küttler, K., Deschl, U., Nakae, D., Gregson, R., Vinlove, M. P., Brix, A. E., Singh, B., Belpoggi, F., and Ward, J. M. (2010) Proliferative and nonproliferative lesions of the rat and mouse hepatobiliary system. *Toxicol. Pathol.* **38**, 5S–81S
20. Smith, Z. D., Gu, H., Bock, C., Gnirke, A., and Meissner, A. (2009) High-throughput bisulfite sequencing in mammalian genomes. *Methods* **48**, 226–232
21. Storey, J. D. (2002) A direct approach to false discovery rates. *J. R. Stat. Soc. Series B (Stat. Methodol.)* **64**, 479–498
22. McLean, C. Y., Bristor, D., Hiller, M., Clarke, S. L., Schaar, B. T., Lowe, C. B., Wenger, A. M., and Bejerano, G. (2010) GREAT improves functional interpretation of cis-regulatory regions. *Nat. Biotechnol.* **28**, 495–501
23. Niculescu, M. D., Lupu, D. S., and Craciunescu, C. N. (2013) Perinatal manipulation of α-linolenic acid intake induces epigenetic changes in maternal and offspring livers. *FASEB J.* **27**, 350–358
24. Zhang, B., Kirov, S., and Snoddy, J. (2005) WebGestalt: an integrated system for exploring gene sets in various biological contexts. *Nucleic Acids Res.* **33**, W741–W748
25. Bennett, B. J., Farber, C. R., Orozco, L., Kang, H. M., Ghazalpour, A., Siemers, N., Neubauer, M., Neuhaus, I., Yordanova, R., Guan, B., Truong, A., Yang, W. P., He, A., Kayne, P., Gargalovic, P., Kirchgessner, T., Pan, C., Castellani, L. W., Kostem, E., Furlotte, N., Drake, T. A., Eskin, E., and Lusis, A. J. (2010) A high-resolution association mapping panel for the dissection of complex traits in mice. *Genome Res.* **20**, 281–290
26. Orozco, L. D., Rubbi, L., Martin, L. J., Fang, F., Hormozdiari, F., Che, N., Smith, A. D., Lusis, A. J., and Pellegrini, M. (2014) Intergenerational genomic DNA methylation patterns in mouse hybrid strains. *Genome Biol.* **15**, R68
27. Ittrich, C., Deml, E., Oesterle, D., Küttler, K., Mellert, W., Brendler-Schwaab, S., Enzmann, H., Schladt, L., Bannasch, P., Haertel, T., Mönnikes, O., Schwarz, M., and Kopp-Schneider, A. (2003) Prevalidation of a rat liver foci bioassay (RLFB) based on results from 1600 rats: a study report. *Toxicol. Pathol.* **31**, 60–79
28. Kakehashi, A., Kato, A., Inoue, M., Ishii, N., Okazaki, E., Wei, M., Tachibana, T., and Wanibuchi, H. (2010) Cytokeratin 8/18 as a new marker of mouse liver preneoplastic lesions. *Toxicol. Appl. Pharmacol.* **242**, 47–55
29. Orozco, L. D., Morselli, M., Rubbi, L., Guo, W., Go, J., Shi, H., Lopez, D., Furlotte, N. A., Bennett, B. J., Farber, C. R., Ghazalpour, A., Zhang, M. Q., Bahous, R., Rozen, R., Lusis, A. J., and Pellegrini, M. (2015) Epigenome-wide association of liver methylation patterns and complex metabolic traits in mice. *Cell Metab.* **21**, 905–917
30. Tatematsu, M., Tsuda, H., Shirai, T., Masui, T., and Ito, N. (1987) Placental glutathione S-transferase (GST-P) as a new marker for hepatocarcinogenesis: *in vivo* short-term screening for hepatocarcinogens. *Toxicol. Pathol.* **15**, 60–68
31. Tsuda, H., Fukushima, S., Wanibuchi, H., Morimura, K., Nakae, D., Imaida, K., Tatematsu, M., Hirose, M., Wakabayashi, K., and Moore, M. A. (2003) Value of GST-P positive preneoplastic hepatic foci in dose-response studies of hepatocarcinogenesis: evidence for practical thresholds with both genotoxic and nongenotoxic carcinogens. A review of recent work. *Toxicol. Pathol.* **31**, 80–86
32. Satoh, K., and Hatayama, I. (2002) Anomalous elevation of glutathione S-transferase P-form (GST-P) in the elementary process of epigenetic initiation of chemical hepatocarcinogenesis in rats. *Carcinogenesis* **23**, 1193–1198
33. Kushida, M., Kamendulis, L. M., Peat, T. J., and Klaunig, J. E. (2011) Dose-related induction of hepatic preneoplastic lesions by diethylnitrosamine in C57BL/6 mice. *Toxicol. Pathol.* **39**, 776–786
34. Kakehashi, A., Inoue, M., Wei, M., Fukushima, S., and Wanibuchi, H. (2009) Cytokeratin 8/18 overexpression and complex formation as an indicator of GST-P positive foci transformation into hepatocellular carcinomas. *Toxicol. Appl. Pharmacol.* **238**, 71–79
35. Clarke, S. (2001) S-Adenosylmethionine-dependent methyltransferases. In *Homocysteine in Health and Disease* (Carmel, R., and Jacobsen, D. W., eds.), pp. 63–78, Cambridge University Press, Cambridge
36. Lin, N., Qin, S., Luo, S., Cui, S., Huang, G., and Zhang, X. (2014) Homocysteine induces cytotoxicity and proliferation inhibition in neural stem cells *via* DNA methylation *in vitro*. *FEBS J.* **281**, 2088–2096
37. Pogribny, I. P., Karpf, A. R., James, S. R., Melnyk, S., Han, T., and Tryndyak, V. P. (2008) Epigenetic alterations in the brains of Fisher 344 rats induced by long-term administration of folate/methyl-deficient diet. *Brain Res.* **1237**, 25–34
38. Pogribny, I. P., Shpyleva, S. I., Muskhelishvili, L., Bagnyukova, T. V., James, S. J., and Beland, F. A. (2009) Role of DNA damage and alterations in cytosine DNA methylation in rat liver carcinogenesis induced by a methyl-deficient diet. *Mutat. Res.* **669**, 56–62
39. Takumi, S., Okamura, K., Yanagisawa, H., Sano, T., Kobayashi, Y., and Nohara, K. (2015) The effect of a methyl-deficient diet on the global DNA methylation and the DNA methylation regulatory pathways. *J. Appl. Toxicol.* **35**, 1550–1556
40. Hansen, K. D., Timp, W., Bravo, H. C., Sabunciyan, S., Langmead, B., McDonald, O. G., Wen, B., Wu, H., Liu, Y., Diep, D., Briem, E., Zhang, K., Irizarry, R. A., and Feinberg, A. P. (2011) Increased methylation variation in epigenetic domains across cancer types. *Nat. Genet.* **43**, 768–775
41. Berman, B. P., Weisenberger, D. J., Aman, J. F., Hinoue, T., Ramjan, Z., Liu, Y., Noushmehr, H., Lange, C. P., van Dijk, C. M., Tollenaar, R. A., Van Den Berg, D., and Laird, P. W. (2011) Regions of focal DNA hypermethylation and long-range hypomethylation in colorectal cancer coincide with nuclear lamina-associated domains. *Nat. Genet.* **44**, 40–46
42. Briggs, M. W., and Sacks, D. B. (2003) IQGAP proteins are integral components of cytoskeletal regulation. *EMBO Rep.* **4**, 571–574

43. Vaitheesvaran, B., Hartil, K., Navare, A., Zheng, P., OBroin, P., Golden, A., Guha, Lee, W., Kurland, I. J., and Bruce, J. E. (2014) Role of the tumor suppressor IQGAP2 in metabolic homeostasis: Possible link between diabetes and cancer. *Metabolomics* **10**, 920–937
44. Schmidt, V. A., Chiariello, C. S., Capilla, E., Miller, F., and Bahou, W. F. (2008) Development of hepatocellular carcinoma in Iqgap2-deficient mice is IQGAP1 dependent. *Mol. Cell. Biol.* **28**, 1489–1502
45. Ni, M., Chen, Y., Fei, T., Li, D., Lim, E., Liu, X. S., and Brown, M. (2013) Amplitude modulation of androgen signaling by c-MYC. *Genes Dev.* **27**, 734–748
46. Guo, X., Wang, M., Zhao, Y., Wang, X., Shen, M., Zhu, F., Shi, C., Xu, M., Li, X., Peng, F., Zhang, H., Feng, Y., Xie, Y., Xu, X., Jia, W., He, R., Jiang, J., Hu, J., Tian, R., and Qin, R. (2016) Par3 regulates invasion of pancreatic cancer cells *via* interaction with Tiam1. *Clin. Exp. Med.* **16**, 357–365
47. Segal, L., Katz, L. S., Lupu-Meiri, M., Shapira, H., Sandbank, J., Gershengorn, M. C., and Oron, Y. (2014) Proteinase-activated receptors differentially modulate *in vitro* invasion of human pancreatic adenocarcinoma PANC-1 cells in correlation with changes in the expression of CDC42 protein. *Pancreas* **43**, 103–108
48. Fernández, A. F., Bayón, G. F., Urdinguio, R. G., Toraño, E. G., García, M. G., Carella, A., Petrus-Reurer, S., Ferrero, C., Martinez-Camblor, P., Cubillo, I., García-Castro, J., Delgado-Calle, J., Pérez-Campo, F. M., Riancho, J. A., Bueno, C., Menéndez, P., Mentink, A., Mareschi, K., Claire, F., Fagnani, C., Medda, E., Toccaceli, V., Brescianini, S., Moran, S., Esteller, M., Stolzing, A., de Boer, J., Nisticò, L., Stazi, M. A., and Fraga, M. F. (2015) H3K4me1 marks DNA regions hypomethylated during aging in human stem and differentiated cells. *Genome Res.* **25**, 27–40
49. Gnatenko, D. V., Xu, X., Zhu, W., and Schmidt, V. A. (2013) Transcript profiling identifies iqgap2(-/-) mouse as a model for advanced human hepatocellular carcinoma. *PLoS One* **8**, e71826
50. Warner, D. R., Pisano, M. M., Roberts, E. A., and Greene, R. M. (2003) Identification of three novel Smad binding proteins involved in cell polarity. *FEBS Lett.* **539**, 167–173
51. Odom, D. T., Zizlsperger, N., Gordon, D. B., Bell, G. W., Rinaldi, N. J., Murray, H. L., Volkert, T. L., Schreiber, J., Rolfe, P. A., Gifford, D. K., Fraenkel, E., Bell, G. I., and Young, R. A. (2004) Control of pancreas and liver gene expression by HNF transcription factors. *Science* **303**, 1378–1381
52. Jiang, S., Minter, L. C., Stratton, S. A., Yang, P., Abbas, H. A., Akdemir, Z. C., Pant, V., Post, S., Gagea, M., Lee, R. G., Lozano, G., and Barton, M. C. (2015) TRIM24 suppresses development of spontaneous hepatic lipid accumulation and hepatocellular carcinoma in mice. *J. Hepatol.* **62**, 371–379
53. Khetchoumian, K., Teletin, M., Tisserand, J., Mark, M., Herquel, B., Ignat, M., Zucman-Rossi, J., Cammas, F., Lerouge, T., Thibault, C., Metzger, D., Chambon, P., and Losson, R. (2007) Loss of *Trim24* (Tif1alpha) gene function confers oncogenic activity to retinoic acid receptor alpha. *Nat. Genet.* **39**, 1500–1506

Received for publication October 25, 2016.
Accepted for publication January 17, 2017.